

Proceedings

Integrating Diphenyl Diselenide and Its MeHg⁺ Detoxificant Mechanism on a Conceptual DFT Framework †

Folorunsho Bright Omage ¹, Cláudia S. Oliveira ¹, Laura Orian ^{2,*}
and Joao Batista Teixeira Rocha ^{1,*}

¹ Departamento de Bioquímica e Biologia Molecular, Universidade Federal de Santa Maria, Santa Maria RS 97105-900, Brazil; omagefolorunsho@gmail.com (F.B.O.); claudia.bioquimica@yahoo.com.br (C.S.O.)

² Dipartimento di Scienze Chimiche, Università degli Studi di Padova, Via Marzolo 1, 35131 Padova, Italy

* Correspondence: Correspondence: laura.orian@unipd.it (L.O.); jbtrocha@gmail.com (J.B.T.R.)

† Presented at the 1st International Electronic Conference on Catalysis Sciences, 10–30 November 2020; Available online: <https://eccs2020.sciforum.net>.

Published: 9 November 2020

Abstract: Methylmercury (MeHg⁺) is an important environmental contaminant and its toxicity is associated with its interaction with selenium (e.g., selenol groups of selenoproteins or HSe⁻, which is the pivotal metabolite for Se incorporation into selenoproteins). We hypothesized that (PhSe)₂ mediated MeHg⁺ detoxification could be indirectly altered by its open or closed conformation. The two conformations of (PhSe)₂ were located on the potential energy surface (PES) computed at ZORA-OPBE-D3(BJ)/ZORA-def2-TZVP level of theory. HPLC analysis indicated that (PhSe)₂ did not react with MeHg⁺, but its reduced intermediate formed a stable complex with MeHg⁺. The nudged elastic band (NEB) method revealed conformational changes from closed to open state with an H⁻ (2 electrons) transfer from NaBH₄, forming a reactant complex-like transition state (TS). The UV-Vis spectrophotometer used in combination with the time-dependent density functional theory (TD-DFT) indicated that the signal of (PhSe)₂ at 239 nm was possibly the open conformer's signal with oscillator strength 0.1 and a $\pi \rightarrow \pi^*$ electron transfer character. The experimental band gap energy of (PhSe)₂ at 5.20 eV matched to the excitation energy of the open conformation. The local softness (*S*⁻) on the selenium atoms almost doubles, as state changes from closed to open. The theoretical results have indicated that the open conformation of (PhSe)₂ is likely the one that reacts with NaBH₄ to form the PhSeH, which can react with MeHg⁺.

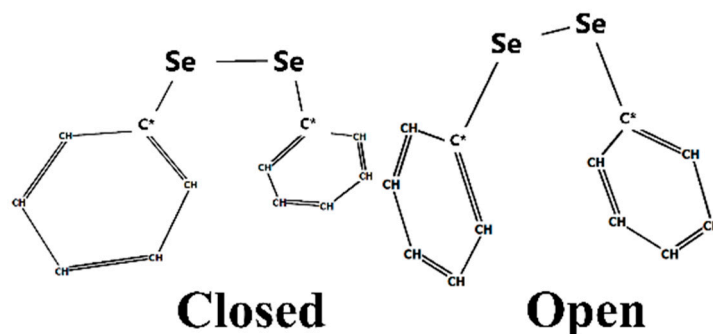
Keywords: diphenyl diselenide; rHPLC; TD-DFT; DFT calculations; conceptual DFT; NEB

1. Introduction

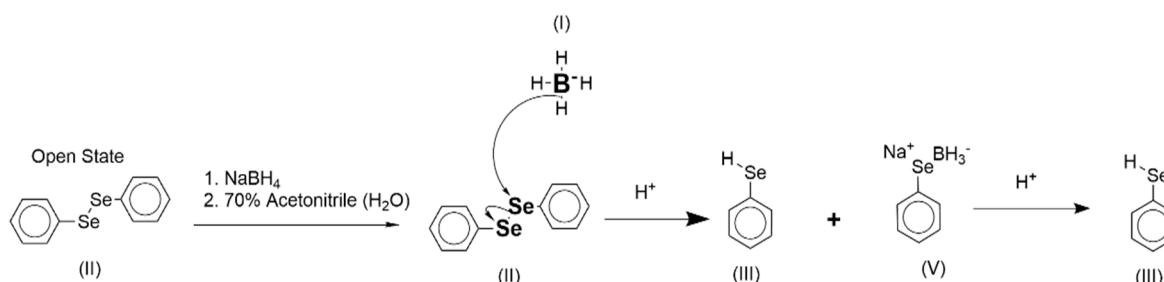
In the aquatic food web, methylmercury (MeHg⁺) can be biomagnified and can reach toxic levels in the edible muscle of predatory or piscivorous fish [1,2]. The frequent consumption of predatory fish can result in MeHg⁺ intoxication [2]. The toxicity of the soft electrophilic MeHg⁺ is mediated by inactivation of proteins containing soft nucleophilic sites (e.g., thiol- and selenol-containing proteins) [3–7]. MeHg⁺ has an extremely high affinity for –SH and –SeH groups [5,8]. Experimental and theoretical studies have indicated that the affinity of MeHg⁺ for –SeH is greater than for –SH groups [5]. Selenium (Se) is an essential element for vertebrates as part of the selenol group present in the selenocysteine residues found in selenoproteins. In a previous study, we demonstrated that diphenyl diselenide (PhSe)₂ decreased the deposition of Hg in mice treated with MeHg⁺. A decreased mercury burden in liver, kidney, cerebrum and cerebellum of mouse was reported in mice treated with (PhSe)₂

[3,4,9]. We have hypothesized that $(\text{PhSe})_2$ could be reduced to its selenol intermediate PhSeH , which formed a complex with MeHg^+ (i.e., PhSeHgMe) [5,9,10]. The reduction of $(\text{PhSe})_2$ and its eventual reaction with methylmercury have several intricate and interesting parts, as reactions may eventually depend on the conformation assumed by $(\text{PhSe})_2$ in the reacting medium [11–13].

$(\text{PhSe})_2$ presents two conformations in its ground state, referred to as the closed and open conformation (Scheme 1) [12,14]. The reduction of $(\text{PhSe})_2$ using NaBH_4 involves a hydride transfer via a likely single-step mechanism [15], Scheme 2. It has been reported [16] that the hydride transfer process is strongly affected by solvent, with the open state acting as the hydride acceptor from the NaBH_4 donor. A likely mechanism is shown in Scheme 2.



Scheme 1. Closed and open conformation of diphenyl diselenide.



Scheme 2. Diphenyl diselenide reduction by NaBH_4 .

The nudged elastic band (NEB) method [17] was used to locate the relevant points on the PES, i.e., the minima and transition states. TD-DFT [18] calculations were performed at ZORA-CAM-B3LYP/zora-def2-TZVP to compute the excitation energies and interpret the experimental spectrum. Then, we used the conceptual density functional theory (c-DFT), [19] which involves the use of DFT, electron density to unravel the reactivity of chemical systems. Particularly, the Fukui function $f(r)$ was computed. This function is the second derivative of energy (E) at a constant external potential, derived by perturbing the chemical system from N to $N + 1$ and N to $N - 1$ [20]. This function indicates the regioselectivity [21], suggesting a region on a molecule where there will be either a nucleophilic or electrophilic attack.

2. Methods

2.1. Experimental

A stock solution of 10 mM was prepared by dissolving 19.6 mg of $(\text{PhSe})_2$ in 6.28 mL of 70% Acetonitrile, from which 5 μL ($(\text{PhSe})_2$ final concentration of 50 μM) was used in the reaction, same concentration applied to NaBH_4 , DTT and MeHg . The UV absorption spectrum of $(\text{PhSe})_2$ was recorded in the region of 220–450 nm with 70% acetonitrile as the solvent using a UV-1800 Shimadzu

spectrophotometer (Shimadzu, Kyoto, Japan). Analysis of methylmercury reaction with $(\text{PhSe})_2$ was performed using a Shimadzu SPD-20A UV/V is Detector (Shimadzu, Kyoto, Japan). CBM-20A communication bus module and DGU-20A5 Degasser prominence high-performance liquid chromatography (HPLC) controlled by the LCSolution software system version 1.22 SP1. Detection was monitored at 239 nm UV wavelength. The separation was achieved on a VerticalTM VertiSep GES C18 HPLC column (4.6×150 mm). The mobile phase used for the analysis of the reaction was at 70% acetonitrile–0.5% phosphoric acid aqueous solution (70:30, *v/v*) with a flow rate of 0.8 mL/min. An injection volume of 50 μL was used. The retention time was approximately 12.5 min for $(\text{PhSe})_2$. The peak areas were used for quantification. The estimated void volume is 1.75 mL and at 0.8 mL/min flow rate gives 2.19 min.

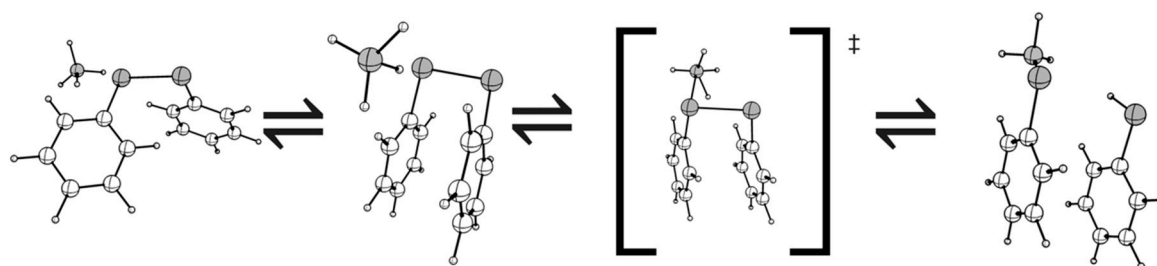
2.2. Computational Methods

All Density Functional Theory (DFT) calculations were done with ORCA 4.1.2 [22,23]. Geometry optimizations and vibrational frequencies were performed at ZORA-OPBE-D3(BJ)/ZORA-def2-TZVP [24,25] level of theory. The Zeroth-order regular approximation (ZORA) was used in order to include scalar relativistic effects due to the presence of selenium atom [26] as previously benchmarked [11]. In addition, the effect of dispersion was included using Grimme's approximation (D3(BJ)) [27,28]. The FMO (frontier molecular orbitals) energies and related parameters were obtained at ZORA-OPBE-D3(BJ)/ZORA-def2-TZVP level. The NEB analysis was carried out at ZORA-OPBE-D3(BJ)/ZORA-def2-TZVP level. The chemical reactivity descriptors used are the local softness (s), global hardness (η) and global softness (S), defined as: $\eta = (\text{IE} - \text{EA})/2$ and $S = 1/(\text{IE} - \text{EA})$ where IE is the Ionization Energy which corresponds to the HOMO energy taken with a negative sign and EA is the electron affinity which corresponds to the LUMO energy taken with a negative sign. The local softness is $s = S (\text{Global Softness}) \times f(r)$ where the Fukui function $f(r)$ [20,29,30] is the second derivative of E at a constant external potential. The dual descriptors $f(2)(r) > 0$ indicate preferable sites for nucleophilic attack and $f(2)(r) < 0$ shows sites for electrophilic attack. The experimental band gap energy was obtained by calculating the energy using the Planck–Einstein relationship $E(\text{eV}) = hc/\lambda$. The pkCSM server [31] (<http://biosig.unimelb.edu.au/pkcsm/prediction>) was used in predicting the total clearance (CL_{tot}) of $(\text{PhSe})_2$, MeHg^+ and MeHgSePh [32].

3. Results

A reactant-like transition state (TS) geometry with the TS energy closer to the reactant complex where the open conformer is present.

The relevant structures of this mechanism are shown in Scheme 3.



Scheme 3. Mechanism of $(\text{PhSe})_2$ reduction.

4. Discussion

The PES scan performed at ZORA-OPBE-D3(BJ)/ZORA-def2-TZVP level of theory across the dihedral angle ψ (C-Se-Se-C *, Scheme 1) reveals two minima corresponding to approximately -80 and $+80$ degrees (Figure 1). The spikes in the curve correspond to switches in the orientation of the phenyl rings converting the open/closed conformations. Solvation brings minimal changes, and the two minima are just slightly shifted, while the phenyl rings orientation in correspondence of these minima is maintained as in the gas phase. The actual detoxifying of MeHg^+ is the selenol metabolite obtained from the reduction of $(\text{PhSe})_2$ by two electrons transfer process (Scheme 2, Figure 3, breaking the Se-Se bond). The orientation of the phenyl rings is expected to modulate the equilibrium shift, either in favor or against the formation of selenol, hence modifying indirectly the detoxification process. Hydride transfer process are strongly affected by solvent [16]. The crystallographic structure retrieved from the Cambridge Structural Database (CSD) [33,34] is in the closed state. At ZORA-CAM-B3LYP/zora-def2-TZVP (Figure 3) the modelled spectrum of the open state, matches to the experimental spectrum at λ_{max} 238.7 nm, with slight difference of only 0.2 nm. The excitation energy of the open state at the same level of theory matches to the experimental band gap energy of 5.2 eV. The cDFT result revealed change in susceptibility of diphenyl diselenide in the closed state for nucleophilic attacks with the dual descriptor $f(2)(r) > 0$ (0.032) to electrophilic attacks with $f(2)(r) = -0.046$, with extended bond length of 5%. Change to open state increases the reactivity, with the local softness (S^-) on the selenium atoms almost doubled.

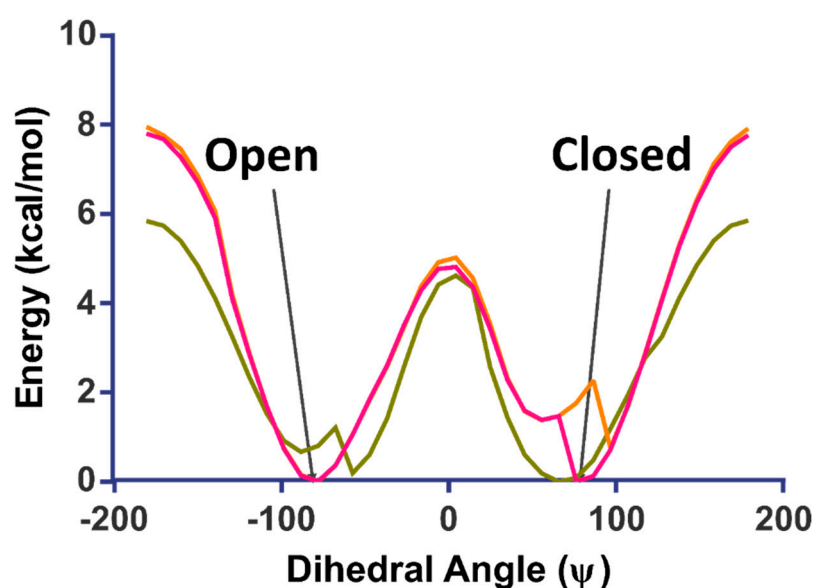


Figure 1. Potential Energy Surface (PES) scan of $(\text{PhSe})_2$. In gas phase (green line) and in different solvents, i.e., chloroform (yellow line) and acetonitrile (pink line); level of theory: ZORA-OPBE-D3(BJ)/ZORA-def2-TZVP.

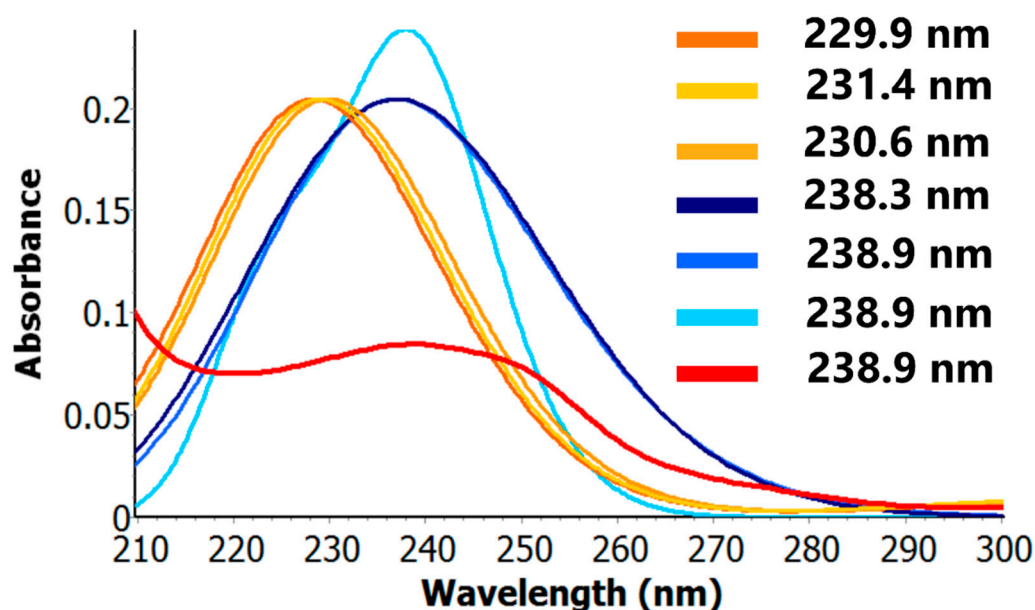


Figure 2. Computed spectra of the closed and open conformers of $(\text{PhSe})_2$ in gas phase (orange and skye blue, respectively) and in different media, i.e. chloroform (light orange and light blue, respectively) and acetonitrile (gold and dark blue, respectively) and experimental spectrum recorded in acetonitrile (red); level of theory: ZORA-CAM-B3LYP/TZVP.

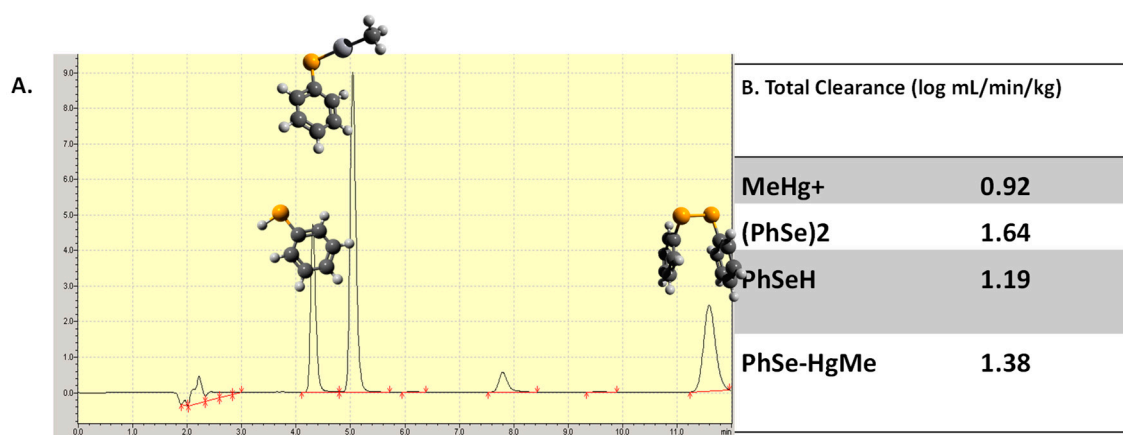


Figure 3. (A). The chromatogram of $(\text{PhSe})_2$ using VerticalTM VertiSep GES C18 HPLC column (4.6×150 mm) with 70% acetonitrile, 0.5% phosphoric acid aqueous solution (70:30, *v/v*) mobile phase at a flow rate of 0.8 mL/min. (B). Total clearance of the reagents as predicted using pKCSM.

5. Conclusions

In this work, we have used both experimental and theoretical approach to identify the reactive state of $(\text{PhSe})_2$. We ascribe the experimental absorption of $(\text{PhSe})_2$ at 239 nm to a dominant open state with a $\pi \rightarrow \pi^*$ electron transfer character. The reaction with MeHg^+ was observed to be preceded by a reduction reaction. A hydride transfer from NaBH_4 to $(\text{PhSe})_2$ open state was postulated and confirmed by a NEB profile: a reactant-like transition state (TS) geometry is present leading to selenol as the product. This study provides new insight into the study of $(\text{PhSe})_2$ use as a methylmercury detoxificant agent.

Author Contributions: Conceptualization, supervision, validation and project administration, J.B.T.R. and L.O.; methodology, J.B.T.R., L.O., F.B.O., C.S.O.; formal analysis, investigation and data curation, F.B.O.; writing—original draft preparation, F.B.O., J.B.T.R., L.O., writing—review and editing, F.B.O., C.S.O., J.B.T.R., L.O. All authors have read and agreed to the published version of the manuscript.

Funding: J.B.T.R., F.B.O., C.S.O. and L.O. would like to thank the financial support by Coordination for Improvement of Higher Education Personnel CAPES/PROEX (n° 23038.005848/2018-31; n° 88887.354370/2019-00), and P-DiSC 2018 MAD3S (Modeling Antioxidant Drugs: Design and Development of computer-aided molecular Systems), the CAPES/PrInt—Institutional Internationalization Project (n° 88887.374997/2019-00), IS CRA Grant MEMES (MEthylMErcury and Selenoproteins), the National Council for Scientific and Technological Development (CNPq), and the Rio Grande do Sul Foundation for Research Support (FAPERGS).

Conflicts of Interest: The authors declare no conflict of interest.

References

1. Farina, M.; Aschner, M. Glutathione antioxidant system and methylmercury-induced neurotoxicity: An intriguing interplay. *Biochim. Biophys. Acta-Gen. Subj.* **2019**, *1863*, 129285, doi:10.1016/j.bbagen.2019.01.007.
2. Farina, M.; Rocha, J.B.T.; Aschner, M. Mechanisms of methylmercury-induced neurotoxicity: Evidence from experimental studies. *Life Sci.* **2011**, *89*, 555–563.
3. Glaser, V.; Moritz, B.; Schmitz, A.; Dafré, A.L.; Nazari, E.M.; Rauh Müller, Y.M.; Feksa, L.; Straliootta, M.R.; De Bem, A.F.; Farina, M. Protective effects of diphenyl diselenide in a mouse model of brain toxicity. *Chem. Biol. Interact.* **2013**, *206*, 18–26, doi:10.1016/j.cbi.2013.08.002.
4. Glaser, V.; Martins, R.D.P.; Vieira, A.J.H.; Oliveira, E.D.M.; Straliootta, M.R.; Mukdsi, J.H.; Torres, A.I.; De Bem, A.F.; Farina, M.; Da Rocha, J.B.T.; et al. Diphenyl diselenide administration enhances cortical mitochondrial number and activity by increasing hemeoxygenase type 1 content in a methylmercury-induced neurotoxicity mouse model. *Mol. Cell. Biochem.* **2014**, *390*, 1–8, doi:10.1007/s11010-013-1870-9.
5. Madabeni, A.; Dalla Tiezza, M.; Omega, F.B.; Nogara, P.A.; Bortoli, M.; Rocha, J.B.T.; Orian, L. Chalcogen-mercury bond formation and disruption in model Rabenstein's reactions: A computational analysis. *J. Comput. Chem.* **2020**, *41*, 2045–2054, doi:10.1002/jcc.26371.
6. Branco, V.; Carvalho, C. The thioredoxin system as a target for mercury compounds. *Biochim. Biophys. Acta-Gen. Subj.* **2019**, *1863*, 129255.
7. Meinerz, D.F.; Branco, V.; Aschner, M.; Carvalho, C.; Rocha, J.B.T. Diphenyl diselenide protects against methylmercury-induced inhibition of thioredoxin reductase and glutathione peroxidase in human neuroblastoma cells: A comparison with ebselen. *J. Appl. Toxicol.* **2017**, *37*, 1073–1081, doi:10.1002/jat.3458.
8. Nogara, P.A.; Oliveira, C.S.; Schmitz, G.L.; Piquini, P.C.; Farina, M.; Aschner, M.; Rocha, J.B.T. Methylmercury's chemistry: From the environment to the mammalian brain. *Biochim. Biophys. Acta-Gen. Subj.* **2019**, *1863*, 129284, doi:10.1016/j.bbagen.2019.01.006.
9. de Freitas, A.S.; Funck, V.R.; dos Santos Rotta, M.; Bohrer, D.; Mörschbacher, V.; Puntel, R.L.; Nogueira, C.W.; Farina, M.; Aschner, M.; Rocha, J.B.T. Diphenyl diselenide, a simple organoselenium compound, decreases methylmercury-induced cerebral, hepatic and renal oxidative stress and mercury deposition in adult mice. *Brain Res. Bull.* **2009**, *79*, 77–84, doi:10.1016/j.brainresbull.2008.11.001.
10. Oliveira, C.S.; Nogara, P.A.; Ardisson-Araújo, D.M.P.; Aschner, M.; Rocha, J.B.T.; Dórea, J.G. Neurodevelopmental Effects of Mercury. *Adv. Neurotoxicol.* **2018**, *2*, 27–86.
11. Zaccaria, F.; Wolters, L.P.; Fonseca Guerra, C.; Orian, L. Insights on selenium and tellurium diaryldichalcogenides: A benchmark DFT study. *J. Comput. Chem.* **2016**, *37*, 1672–1680, doi:10.1002/jcc.24383.
12. Bortoli, M.; Tiezza, M.D.; Muraro, C.; Saielli, G.; Orian, L. The ¹²⁵Te chemical shift of diphenyl ditelluride: Chasing conformers over a flat energy surface. *Molecules* **2019**, *24*, 1250, doi:10.3390/molecules24071250.
13. Piccoli, B.C.; Alvim, J.C.; da Silva, F.D.; Nogara, P.A.; Olagoke, O.C.; Aschner, M.; Oliveira, C.S.; Rocha, J.B.T. High level of methylmercury exposure causes persisted toxicity in *Nauphoeta cinerea*. *Environ. Sci. Pollut. Res.* **2020**, *27*, 4799–4813, doi:10.1007/s11356-019-06989-9.
14. Bortoli, M.; Zaccaria, F.; Tiezza, M.D.; Bruschi, M.; Guerra, C.F.; Matthias Bickelhaupt, F.; Orian, L. Oxidation of organic diselenides and ditellurides by H₂O₂ for bioinspired catalyst design. *Phys. Chem. Chem. Phys.* **2018**, *20*, 20874–20885, doi:10.1039/c8cp02748j.
15. Powell, M.F.; Bruice, T.C. Hydride vs. Electron Transfer in the Reduction of Flavin and Flavin Radical by 1,4-Dihydropyridines. *J. Am. Chem. Soc.* **1983**, *105*, 1014–1021.

16. Hori, Y.; Ida, T.; Mizuno, M. A comparative theoretical study of the hydride transfer mechanisms during LiAlH₄ and LiBH₄ reductions. *Comput. Theor. Chem.* **2016**, *1076*, 86–93, doi:10.1016/j.comptc.2015.12.014.
17. Jónsson, H.; Mills, G.; Jacobsen, K.W. *Nudged Elastic Band Method for Finding Minimum Energy Paths of Transitions*. Classical and Quantum Dynamics in Condensed Phase Simulations, ed. B. J. Berne et al. (World Scientific, Singapore), 1998.
18. Runge, E.; Gross, E.K.U. Density-functional theory for time-dependent systems. *Phys. Rev. Lett.* **1984**, *52*, 997, doi:10.1103/PhysRevLett.52.997.
19. Parr, R.G.; Yang, W. Density Functional Approach to the Frontier-Electron Theory of Chemical Reactivity. *J. Am. Chem. Soc.* **1984**, *106*, 4049–4050, doi:10.1021/ja00326a036.
20. Méndez, F.; Gázquez, J.L. Chemical Reactivity of Enolate Ions: The Local Hard and Soft Acids and Bases Principle Viewpoint. *J. Am. Chem. Soc.* **1994**, *116*, 9298–9301, doi:10.1021/ja00099a055.
21. Berger, G. Using conceptual density functional theory to rationalize regioselectivity: A case study on the nucleophilic ring-opening of activated aziridines. *Comput. Theor. Chem.* **2013**, *1010*, 11–18, doi:10.1016/j.comptc.2012.12.029.
22. Neese, F. The ORCA program system. *Wiley Interdiscip. Rev. Comput. Mol. Sci.* **2012**, *21*, 73–78, doi:10.1002/wcms.81.
23. Neese, F. The ORCA Program System: Software Update—Version 4.0. *Wiley Interdiscip. Rev. Comput. Mol. Sci.* **2018**, doi:10.1002/wcms.1327.
24. Swart, M.; Ehlers, A.W.; Lammertsma, K. Performance of the OPBE exchange-correlation functional. *Mol. Phys.* **2004**, *102*, 2467–2474, doi:10.1080/0026897042000275017.
25. Weigend, F.; Ahlrichs, R. Balanced Basis Sets of Split Valence, Triple Zeta Valence and Quadruple Zeta Valence. *Phys. Chem. Chem. Phys.* **2005**, *7*, 3297–3305, doi:10.1039/b508541a.
26. Van Lenthe, E.; Baerends, E.J.; Snijders, J.G. Relativistic total energy using regular approximations. *J. Chem. Phys.* **1994**, *101*, 9783–9792, doi:10.1063/1.467943.
27. Grimme, S.; Ehrlich, S.; Goerigk, L. Effect of the Damping Function in Dispersion Corrected Density Functional Theory. *J. Comput. Chem.* **2011**, *32*, 1456–1465, doi:10.1002/jcc.
28. Nguyen, M.T.; Creve, S.; Eriksson, L.A.; Vanquickenborne, L.G. Calculation of the hyperfine constants of phosphorus-containing radicals. **1997**, *91*, 537–550.
29. Roos, G.; Geerlings, P.; Messens, J. Enzymatic catalysis: The emerging role of conceptual density functional theory. *J. Phys. Chem. B* **2009**, *113*, 13465–13475, doi:10.1021/jp9034584.
30. Fukui, K. The Path of Chemical Reactions—The IRC Approach. *Acc. Chem. Res.* **1981**, *14*, 363–368, doi:10.1021/ar00072a001.
31. Pires, D.E.V.; Blundell, T.L.; Ascher, D.B. pkCSM: Predicting small-molecule pharmacokinetic and toxicity properties using graph-based signatures. *J. Med. Chem.* **2015**, *58*, 4066–4072, doi:10.1021/acs.jmedchem.5b00104.
32. Wilkinson, G.R. Clearance approaches in pharmacology. *Pharmacol. Rev.* **1987**, *39*, 1–47.
33. Allen, F.H. The Cambridge Structural Database: A quarter of a million crystal structures and rising. *Acta Crystallogr. Sect. B Struct. Sci.* **2002**, 380–388.
34. Groom, C.R.; Bruno, I.J.; Lightfoot, M.P.; Ward, S.C. The Cambridge structural database. *Acta Crystallogr. Sect. B Struct. Sci. Cryst. Eng. Mater.* **2016**, *72*, 171–179, doi:10.1107/S2052520616003954.

Publisher's Note: MDPI stays neutral with regard to jurisdictional claims in published maps and institutional affiliations.



© 2020 by the authors. Licensee MDPI, Basel, Switzerland. This article is an open access article distributed under the terms and conditions of the Creative Commons Attribution (CC BY) license (<http://creativecommons.org/licenses/by/4.0/>).